Track–Stair Interaction Analysis and Online Tipover Prediction for a Self-Reconfigurable Tracked Mobile Robot Climbing Stairs

Yugang Liu and Guangjun Liu, *Senior Member, IEEE*

***Abstract*—This paper analyzes track–stair interactions and develops an online tipover prediction algorithm for a self-reconfigurable tracked mobile robot climbing stairs, which is vulnerable to tipping-over. Tipover prediction and prevention for a tracked mobile robot in stair climbing are intractable problems because of the complex track–stair interactions. Unlike the wheeled mobile robots, which are normally assumed to obey the nonholonomic constraints, slippage is unavoidable for a tracked mobile robot, especially in stair climbing. Furthermore, the track–stair interactive forces are complicated, which may take the forms of grouser-tread hooking force, track–stair edge frictional force, grouser-riser clutching force, and even their compositions. In this paper, the track–stair interactions are analyzed systematically, and tipover stability criteria are derived for a tracked mobile robot climbing stairs. An online tipover prediction algorithm is also developed, which forms an essential part for autonomous and semiautonomous stair-climbing control. The effectiveness of the proposed algorithms are verified by experiments.**

***Index Terms*—Stair climbing, tipover prediction, tracked mobile robot, track–stair interactions.**

I. Introduction

TRACKED vehicles have attracted attentions from numerous researchers in recent years since they provide better floatation and traction than the wheeled ones, and this characteristic brings them substantial application potentials in explosive ordnance disposing, searching, rescuing, mining, logging, farming, earth moving, and planetary exploring among others. Traditionally, most of the tracked vehicles were designed to be bulky and heavy to suit for field operations on natural terrain. Nowadays, robots are getting closer to human beings, and many lightweight tracked mobile robots are developed for artificial environments, including stairways.

As one of the most omnipresent artificial environments, stairway represents a serious challenge to robotics, which has to be addressed for robots to operate efficiently in urban environments. According to the difference in locomotion type, stair-climbing robots can be categorized into tracked robots [1], [2], wheeled robots [3], legged robots [4], and hybrid robots [5]. With the popularity of modular and reconfigurable robots, more and more efforts are being made in mechanical design to solve the stair-climbing problem, such as the linkage mechanism actuator (LMA) tracked vehicle [1], the tracked reconfigurable modular robot [2], the reconfigurable wheel-legged robot [5], and the Millibot trains [6].

In related research works on stair climbing with tracked vehicles, an autonomous stair-climbing algorithm is developed for Engineering Service, Inc., (ESI) LMA, and the relevant technical problems are identified and analyzed [1]. The stair-climbing process is divided into three steps in terms of riser climbing, riser crossing, and nose-line climbing, and the effects of design parameters on stair-climbing performance are analyzed in [2]. An autonomous stair-climbing algorithm is proposed by utilizing an extended Kalman filter (EKF) to estimate the rotational velocity measurements provided by a three-axial gyroscope and the line parameters acquired from stair edges' projection on a camera image, and extensive experimental results were presented on iRobot PackBot [7]. The drift of heading angle can cause tumbling of a tracked mobile robot climbing stairs. A feedback system is developed for automatic heading control to stabilize stair climbing and its effectiveness is verified using a Remotec Andros mobile robot [8].

On tipover prediction and prevention, several tipover stability criteria have been put forward, such as the zero moment point (ZMP) method [9], the force-angle measure [10], and the supporting force criterion [11]. An online tipover prediction algorithm is proposed and the robot is controlled to return back to the initial configuration in case of tipover instability [12]. A real-time tipover prevention algorithm is developed for redundant nonholonomic mobile modular manipulators by online adjusting self-motions, so that the primary task at the end-effector can be unaffected [13].

Tipover stability is studied without considering track–stair interactions in [1]. A practical method is proposed for evaluating the design parameters off-line in [2], but it does not suit for online tipover prediction. As is well known, slippage is almost unavoidable for a tracked mobile robot while climbing stairs. However, to the best knowledge of the authors, this important issue has never been addressed in the literature. In this paper, the track–stair interactions, including slippage of a self-reconfigurable tracked mobile robot (SRTMR) in stair climbing are analyzed systematically. In that slippage

Manuscript received May 20, 2008; revised July 21, 2008. First published March 27, 2009; current version published September 2, 2009. Recommended by Technical Editor I-M. Chen. This work was supported in part by the Canada Research Chair Program and in part by the Natural Sciences and Engineering Research Council (NSERC) of Canada. This paper was presented in part at the 2008 IEEE Conference on Automation Science and Engineering, Washington, DC, August 23–26.

The authors are with the Department of Aerospace Engineering, Ryerson University, Toronto, ON M5B 2K3, Canada (e-mail: ygliu@ryerson.ca; gjliu@ryerson.ca).

Color versions of one or more of the figures in this paper are available online at http://ieeexplore.ieee.org.

Digital Object Identifier 10.1109/TMECH.2009.2005635

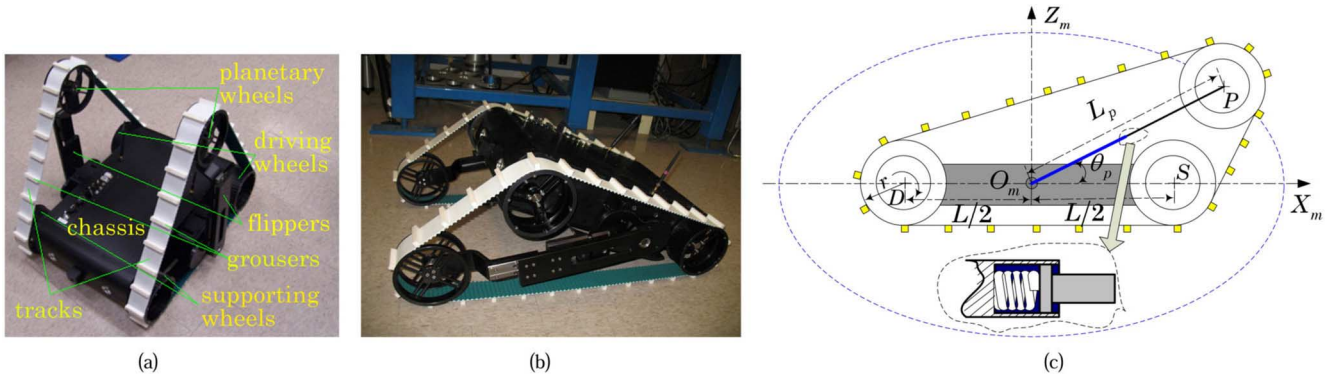

Fig. 1. Self-reconfigurable tracked mobile robot—RLMA. (a) Flippers are raised. (b) Flippers rotate downwards. (c) Spring-loaded prismatic joint.

and track–terrain interactive motions are not considered in the existing tipover stability criteria, we derive new tipover criteria for SRTMRs climbing stairs, with consideration of track–stair interactions. Furthermore, an online tipover prediction algorithm is developed on the basis of the proposed tipover stability criteria.

The remainder of this paper is organized as follows. In Section II, a general procedure for an SRTMR to climb stairs is presented based on a tracked mobile robot in our laboratory. Firm-hooking, firm-clutching, and nonslipping conditions are derived, and slippage as well as track–stair interactive motions are analyzed systematically in Section III. Track–stair interactive forces are analyzed for the SRTMR climbing stairs in Section IV. tipover stability criteria are defined for the SRTMR climbing stairs with consideration of track–stair interactions, and an online tipover prediction algorithm is developed in Section V. To verify the effectiveness of the proposed algorithms, experimental results are presented in Section VI. Finally, concluding remarks are given in Section VII.

II. General Procedure for Stair Climbing

A. SRTMR—RLMA

The SRTMR under investigation is a Ryerson Linkage Mechanism Actuator (RLMA), which is a customized product made by ESI [14]. RLMA consists of a chassis, two tracks, two driving wheels, two supporting wheels, and two planetary wheels, as shown in Fig. 1(a). The two driving wheels can be controlled independently to realize steering; the two planetary wheels are attached at the tip of the flippers; and the two flippers, which are installed at the flanks of the chassis, are driven by one motor (pitch motor) to ensure synchronization of the two tracks. To retain tension in each track, the flippers are equipped with spring-loaded prismatic joints, as shown in Fig. 1(c). The tracks are equipped with grousers, which are designed to improve the stair-climbing ability of RLMA, as shown in Fig. 1.

The motion of the flippers can change the tracks configuration so as to surmount obstacles or climb stairs. According to the position of the flippers and the planetary wheels, RLMA can take three different configurations: if $0 < \theta_p < \pi$, the flippers and the planetary wheels will be raised, as shown in Fig. 1(a); if $\theta_p = 0$ (or $\theta_p = \pi$), the flippers and planetary wheels will be put forward (or backward), and RLMA can achieve the maximum contact area with the terrain; otherwise, if the flippers rotate downward, i.e., $-(\pi/2) \le \theta_p < 0$ [or $\pi < \theta_p < (3\pi/2)$], the supporting wheels (or driving wheels) will be raised and the chassis will be tilted, as shown in Fig. 1(b).

From the earlier analysis, we can see that RLMA has quite good dexterity. However, tipover stability becomes a concerning issue because the reconfiguration of RLMA has dramatic influence on the load distribution. If properly controlled, the reconfiguration of RLMA can be used to balance the load distribution; on the other hand, improper operations may lead to tumbling of the robot from the stairs, which may damage the equipment. Therefore, the development of an effective and reliable tipover prediction algorithm is essential.

B. General Procedure for RLMA Climbing Stairs

To suit different stairway dimensions, RLMA need identify stair parameters. Stair height is identified at the beginning: RLMA is driven to access the first stair with the front part of the tracks vertical to the lower floor until the two tracks touch the riser of the first stair; then, RLMA moves backward for a distance d_0, and the flippers rotate to the front until it touches the edge of the first stair, as shown in Fig. 2(a). By recording the pitch joint angle θ_{p0}, the stair height h can be estimated, which will be detailed in Section II-C. The aforementioned operations belong to planar motion, which is not studied in this paper. The stair-climbing procedure followed can be broken down into four steps, namely "climbing onto the stairs and setting back the flippers," "climbing onto the stairs with the flippers in the back," "going on the nose line," and "landing on the upper floor," as shown in Fig. 2.

Step 1: Climbing onto the stairs and setting back the flippers. To climb onto the first stair, RLMA is driven by the tractive force on the lower level and track–stair interactive forces, as shown in Fig. 2(a) and (b). When the pitch angle of the chassis, which can be read from the three-axis compass, reaches θ_0 (30° in this paper), the driving motors are stopped, as shown in Fig. 2(b). The flippers are rotated clockwise such that it touches the edge of the second stair, as shown in Fig. 2(c). By recording the pitch joint angle θ_{p1}, the tread width b can be identified, which will be detailed in Section II-C. Furthermore, the incline angle of the

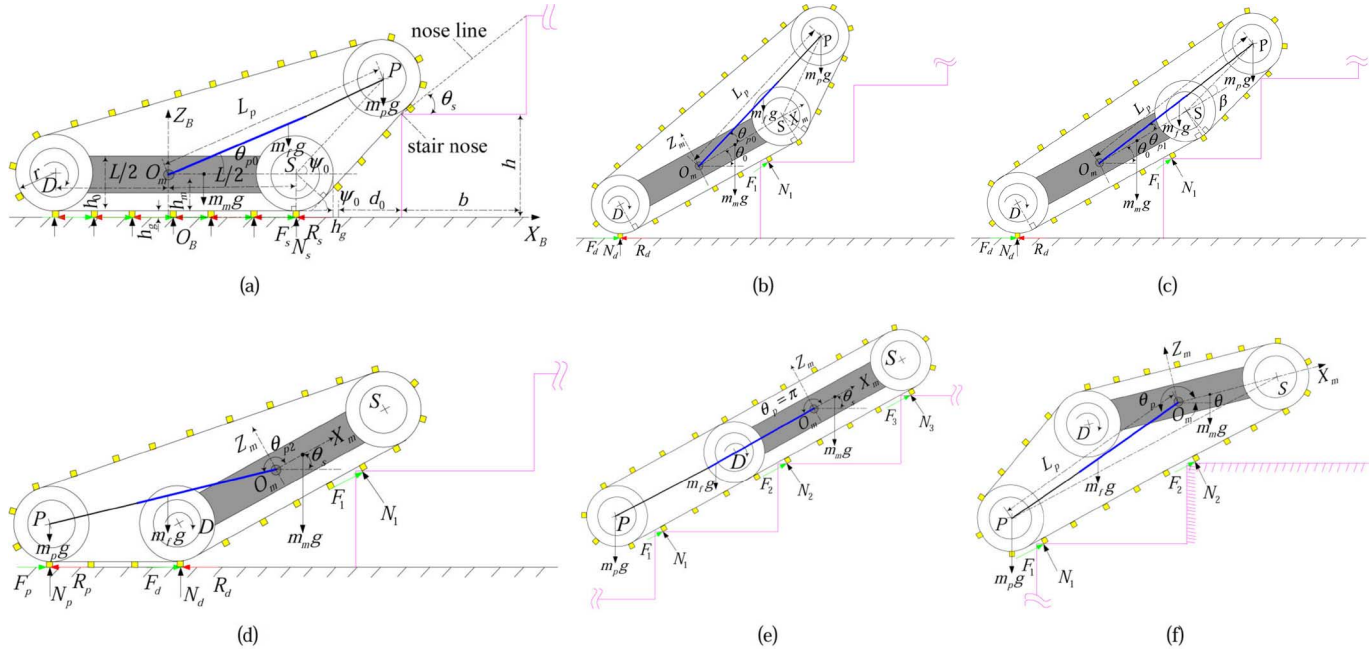

Fig. 2. General procedure for an SRTMR climbing stairs. (a) Touching the first stair edge. (b) Climbing onto the first stair. (c) Putting the flippers forward. (d) Setting back the flippers. (e) Moving on the nose line. (f) Landing on the upper floor.

stairs θ_s can be calculated. Then, the pitch motor is adjusted to recover the original configuration, i.e., $\theta_p = \theta_{p0}$, and the driving motors are adjusted to let $\theta = \theta_s$. To climb the stairs effectively, the flippers are set back to put the robot's center of gravity (COG) forward, as shown in Fig. 2(d).

Step 2: Climbing onto the stairs with the flippers in the back. RLMA climbs onto the stairs again with the flippers and planetary wheels in the back, as shown in Fig. 2(d) and (e). The pitch motor rotates anticlockwise during the course of this climbing to let the chassis parallel to the nose line. There are both tractive force and track–stair interactive forces in step 2.

Step 3: Going on the nose line. For nose-line climbing, the pitch joint is locked at the position $\theta_p = \pi$, and the planetary wheels work as supporting wheels, as shown in Fig. 2(e). RLMA is driven by the track–stair interactive forces in step 3.

Step 4: Landing on the top floor. After the center of the chassis passing over the edge of the last stair, the pitch joint rotates anticlockwise to a definite position (e.g., $\theta_{p2} = 200^\circ$), as shown in Fig. 2(f). Then the driving motors continue to drive RLMA until it plunges onto the upper level. The motion that follows belongs to planar motion, and is not studied in this paper.

Remark 1: The tracked mobile robot under consideration can be controlled manually by the remote controller, which can help eliminate the initial heading error, θ_0 can be adjusted in step 1 if necessary, or θ_{p2} can be adjucted in step 4 to ensure safe landing. The grousers help correct the heading angle because the gravitational force tends to drive the grousers parallel to the edge of the stairs. Certainly, the feedback heading controller presented in [8] would be a good alternative if the drift of heading angle cannot be suppressed effectively with the aforementioned measures under some special situations.

C. Stair-Parameters Identification

From Fig. 1(c), the trajectory of planetary wheel centers is an ellipse, and the flippers' length can be determined by

$$L_p(\theta_p) = \frac{L_p(0)\, L_p(\pi/2)}{\sqrt{L_p^2(\pi/2)\cos^2\theta_p + L_p^2(0)\sin^2\theta_p}} \tag{1}$$

where $L_p(0)$ and $L_p(\pi/2)$ can be determined by the track length L_t and the wheel radius r by $L_p(0) = (L_t - L - 2\pi r)/2$ and $L_p(\pi/2) = (\sqrt{(L_t - 2\pi r - 2L)(L_t - 2\pi r)}/2)$, respectively.

In Fig. 2(a), the incline angle of the track segment between the supporting and planetary wheels ψ_0 can be determined by applying the sine's theorem to the triangle $O_m SP$ as follows:

$$\frac{L/2}{\sin(\psi_0 - \theta_{p0})} = \frac{L_p(\theta_{p0})}{\sin(\pi - \psi_0)} \tag{2}$$

where L is the distance between the supporting and driving wheels, as shown in Figs. 1(c) and 2(a).

Furthermore, the stair height can be calculated from Fig. 2(a) as follows:

$$h = h_g + \left[(d_0 + r + h_g) - r\tan\frac{\psi_0}{2}\right]\tan\psi_0 \tag{3}$$

where h_g is the grousers' height and r is the radius of the wheels.

In Fig. 2(c), the difference between the incline angle of the stairs and that of the chassis can be determined by applying sine's theorem to $O_m SP$ as follows:

$$\frac{L_p(\theta_{p1})}{\sin\beta} = \frac{L/2}{\sin(\beta - \theta_{p1})}. \tag{4}$$

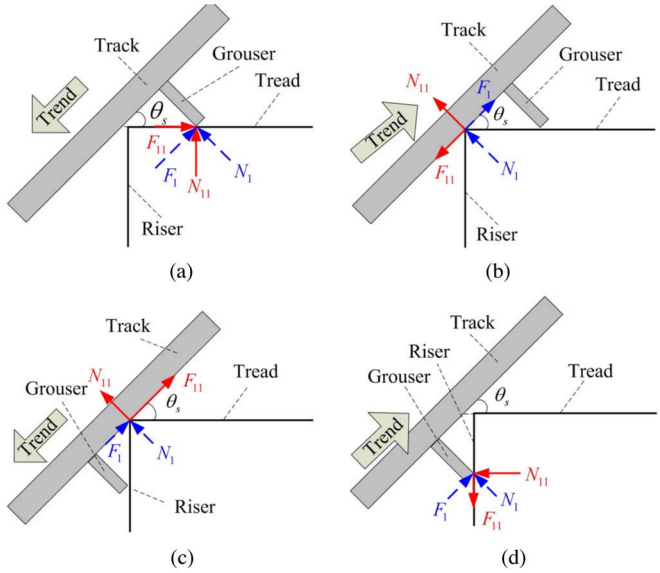

Fig. 3. Track–stair interactive force analysis. F_1 and N_1 represent the equivalent tractive and supporting forces; F_{11} and N_{11} denote actual forces generated at the grouser-tread (riser) or track–stair edge contact points; the hollow arrows show the moving trend of the track. (a) Hooking the tread: $F_1 > -N_1 \cot\theta_s$. (b) Leaving from the tread: $F_1 \le 0$. (c) Leaving from the riser: $F_1 \ge 0$. (d) Clutching the riser: $F_1 < N_1 \tan\theta_s$.

Furthermore, the tread width can be calculated as follows:

$$b = \{2h - [h_g + r + L\sin\theta_0 - r\cos(\beta+\theta_0)]\}\cot(\beta+\theta_0) + r\sin(\beta+\theta_0) + L\cos\theta_0 - r\tan\frac{\theta_0}{2} - (h-h_g)\cot\theta_0. \tag{5}$$

With the stair height h and tread width b identified, the incline angle of the stairs can be easily determined as follows:

$$\theta_s = \arctan\left(\frac{h}{b}\right). \tag{6}$$

III. Slippage and Track–Stair Interactive Motions

In this section, the firm-hooking, firm-clutching, and nonslipping conditions are derived, and the slippage as well as track–stair interactive motions are analyzed for tracked mobile robots climbing stairs. To simplify the calculations, the tracked mobile robot is assumed to be laterally symmetrical and the wheel-track slippage is assumed to be negligible. The stretch of the tracks in stair climbing is assumed to be negligible, and the study on flexible tracks is beyond the scope of this paper. Furthermore, the grousers are assumed to be rigid.

A. Firm-Hooking, Firm-Clutching, and Nonslipping Conditions

The interactive forces between the tracks and the stairs are complicated, which can take the forms of grouser-tread hooking, as shown in Fig. 3(a), track–stair edge friction, as shown in Fig. 3(b) and (c), grouser-riser clutching, as shown in Fig. 3(d), and even their compositions. In Fig. 3(b) and (c), the track works in the same way as pure track without grousers, and the sufficient and necessary condition for nonslipping can be given by $-f_s \le (F_1/N_1) \le f_s$, where f_s is the coefficient of static friction, and the track–stair interactive forces F_1 and N_1 will be derived in Section IV.

From Fig. 3(a), the sufficient and necessary firm-hooking condition can be given by

$$-f_s \le \frac{F_{11}}{N_{11}} = \frac{F_1\cos\theta_s - N_1\sin\theta_s}{F_1\sin\theta_s + N_1\cos\theta_s} \le f_s \tag{7}$$

where $N_1 > 0$, $F_1 > -N_1\cot\theta_s$, and θ_s represents the angle between the track and the stair treads.

Similarly, the sufficient and necessary condition for firm clutching, as shown in Fig. 3(d), can be given by

$$-f_s \le -\frac{F_{11}}{N_{11}} = \frac{F_1\sin\theta_s + N_1\cos\theta_s}{N_1\sin\theta_s - F_1\cos\theta_s} \le f_s \tag{8}$$

where $N_1 > 0$ and $F_1 < N_1\tan\theta_s$.

If $f_s < \cot\theta_s$, solving (7) yields

$$\frac{\sin\theta_s - f_s\cos\theta_s}{\cos\theta_s + f_s\sin\theta_s} \le \frac{F_1}{N_1} \le \frac{\sin\theta_s + f_s\cos\theta_s}{\cos\theta_s - f_s\sin\theta_s}. \tag{9}$$

On the other hand, if $f_s \ge \cot\theta_s$, we can only obtain the left half part of (9).

If $f_s < \tan\theta_s$, solving (8) yields

$$-\frac{\cos\theta_s + f_s\sin\theta_s}{\sin\theta_s - f_s\cos\theta_s} \le \frac{F_1}{N_1} \le \frac{f_s\sin\theta_s - \cos\theta_s}{\sin\theta_s + f_s\cos\theta_s}. \tag{10}$$

Furthermore, the left half part of (10) can be set free on the condition that $f_s \ge \tan\theta_s$.

Remark 2: From the earlier analysis, we can see that the grouser can always hook the tread of the stair firmly to avoid sliding down on the condition that $f_s \ge \cot\theta_s$; even if $f_s < \cot\theta_s$, the track–stair engagement has been improved dramatically than the track without grousers since $(\sin\theta_s + f_s\cos\theta_s)/(\cos\theta_s - f_s\sin\theta_s) \gg f_s$. Similarly, the grouser can always clutch the riser firmly to avoid sliding up on the condition that $f_s \ge \tan\theta_s$; even if $f_s < \tan\theta_s$, the track–stair engagement can also be improved over the track without grousers due to $-(\cos\theta_s + f_s\sin\theta_s)/(\sin\theta_s - f_s\cos\theta_s) \ll -f_s$. This remark explains how grousers can help to improve the stair-climbing ability.

B. Slippage and Interactive Motion Analysis

On the basis of the firm-hooking, firm-clutching, and nonslipping condition analysis, the slippage and track–stair interactive motions can be derived for the first two steps of stair climbing, as shown in Fig. 4, where d_g represents the distance between two adjacent grousers.

In steps 3 and 4, the interactive forces can only be in the form of Fig. 3(a) and (c) or their compositions because $\sum_{i=1}^{n} F_i$ keeps positive; and slippage is still almost unavoidable even if the grouser can hook the tread firmly due to the alternation of hooking points.

If $\{\sum_{i=1}^{n} F_i\}/\{\sum_{i=1}^{n} N_i\} \le f_s$, RLMA can always go on the stairs without slippage, even without grousers. On the other hand, if $\{\sum_{i=1}^{n} F_i\}/\{\sum_{i=1}^{n} N_i\} > f_s$ and if the firm-hooking

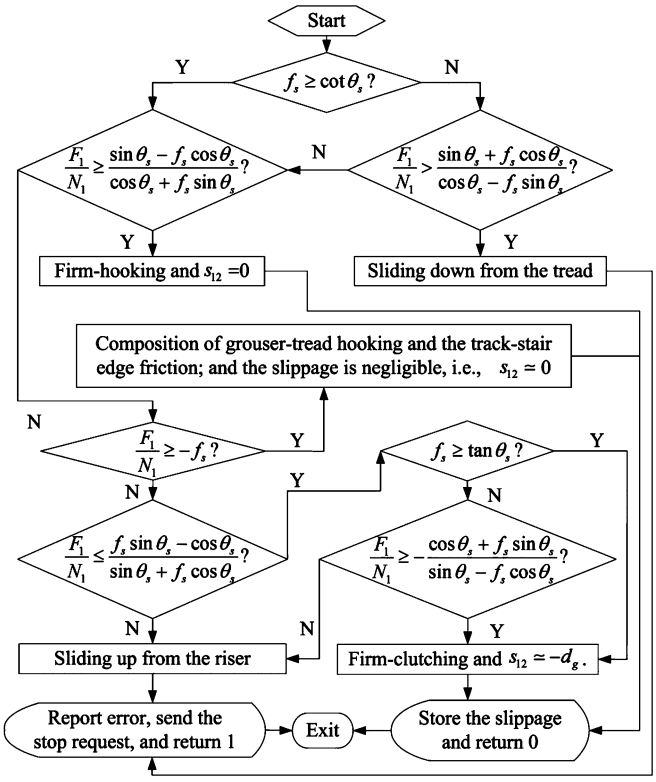

Fig. 4. Slippage and interactive motion analysis for the first two steps.

condition given by (9) can be ensured, slippage may occur only at the beginning of step 3. Otherwise, the track will slide down from the treads, and the stair-climbing process has to be terminated. In the following, we will analyze the slippage of the track in step 3 on the condition that the grousers can hook the treads firmly. Let $\lceil\star\rceil$ denote the ceil function, which gives the smallest integer larger than or equal to "$\star$"; define $k_{\rm rem} = \lceil(\sqrt{b^2+h^2}/d_g)\rceil - (\sqrt{b^2+h^2}/d_g)$, the slippage at the beginning of step 3 can be determined by

$$s_{3,0} = \begin{cases} 0, & \Sigma s_{12} = 0 \\ d_g\, k_{\rm rem}, & \Sigma s_{12} \neq 0 \quad \text{and} \quad k_{\rm rem} \neq 0 \\ d_g, & \Sigma s_{12} \neq 0 \quad \text{and} \quad k_{\rm rem} = 0 \end{cases} \tag{11}$$

where Σs_{12} is the total slippage that occurred in the first two steps.

In view of the grousers interacting with the stairs in the same way as that between gear teeth and racks, the slippage of the track when a grouser releases from the kth stair $s_{3,k}$ can be derived as follows.

1) If $\{k_{\rm rem} = 0\} \cup \{k_{\rm rem} = 1/2\}$, there is no slippage when a grouser releases from the tread of the kth stair, i.e., $s_{3,k} = 0$.
2) If $0 < k_{\rm rem} < 1/2$, when one grouser releases from the kth stair, another grouser will hook the $(k+1)$th one, and the slippage in such a small duration is $s_{3,k,1} = d_g\, k_{\rm rem}$.
3) If $1/2 < k_{\rm rem} < 1$, when one grouser releases from the kth stair, another grouser will hook the $(k+2)$th one, and the slippage in such a small duration can be calculated as $s_{3,k,2} = \left\lceil(2\sqrt{b^2+h^2}/d_g)\right\rceil d_g - 2\sqrt{b^2+h^2}$.

Remark 3: It is observed from experiments that RLMA will slide down if one grouser partially hooks the edge of a stair. Hence, the incomplete hooking phenomenon is not taken into account, and the slippage as well as the turn angle difference caused by hooking point difference are not considered either.

IV. Track–Stair Interactive Force Analysis

A. Kinematics Analysis and Step Classification

The coordinate system is defined as follows: an inertial base frame O_B–$X_B Y_B Z_B$ is fixed on the plane of the lower level, and a frame O_m–$X_m Y_m Z_m$ is attached to RLMA, as shown in Fig. 2(a). In frame O_m–$X_m Y_m Z_m$, O_m is selected as the geometry center of RLMA and $O_m Z_m$ is selected to be vertical with RLMA. Then, the motion of the tracked mobile robot in stair climbing can be determined by the position $O_m(x_m, z_m)$ and the turn angle θ. Furthermore, $O_B Z_B$ is selected to be consistent with the initial position of $O_m Z_m$.

The rotating angles for the two driving wheels should be the same in stair climbing to avoid drift of heading angle. Let the rotating angle of the driving wheels be ϕ, which is set as zero at the beginning of stair climbing. From Fig. 2(a) and (b), we can obtain

$$\begin{aligned} x_m &= r\phi - s_{12} - \frac{L}{2}(1-\cos\theta) \\ z_m &= r + h_g + \frac{L}{2}\sin\theta \\ \theta &= \pi - \arcsin\left\{\frac{L + d_0 + r + h_g - (r\,\phi - s_{12})}{\sqrt{x_{10}^2 + z_{10}^2}}\right\} \\ &\quad - \arctan 2\{x_{10}, z_{10}\} \end{aligned} \tag{12}$$

where $0 \leq \theta \leq \theta_s$, with θ_s representing incline angle of the stairs, $x_{10} = L + d_0 + h_g + r - (r\phi - s_{12})\cos\psi_0$, $z_{10} = (r\phi - s_{12})\sin\psi_0 - (h - h_g - r)$, and $0 \leq \phi \leq \phi_{20} = (L + d_0 + h_g + r - r\tan(\theta_s/2) - (h - h_g)\cot\theta_s + s_{12})/r$ for step 1.

According to the number of track–stair interactive points, step 2 is divided into one-point and two-point subprocesses. Assuming that the change of the chassis's turn angle in step 2 is negligible, from Fig. 2(d), we can obtain the kinematics of the tracked vehicle in step 2 as follows:

$$\begin{aligned} x_m &= x_{20} + \{r(\phi - \phi_{20}) - [s_{12}(\phi) - s_{12}(\phi_{20})]\}\cos\theta \\ z_m &= z_{20} + \{r(\phi - \phi_{20}) - [s_{12}(\phi) - s_{12}(\phi_{20})]\}\sin\theta \end{aligned} \tag{13}$$

where $x_{20} = d_0 + h_g + r + (L(1+\cos\theta_s)/2) - r\tan(\theta_s/2) - (h - h_g)\cot\theta_s$ and $z_{20} = r + h_g + (L/2)\sin\theta_s$.

From (13) and Fig. 2(d), the necessary condition for RLMA to be in the one-point subprocess of step 2 can be derived as

$$\phi_{20} < \phi < \phi_{21} \tag{14}$$

where $\phi_{21} = (2h - r - h_g + r\cos\theta_s - L\sin\theta_s)/r\sin\theta_s + (s_{12}(\phi) - s_{12}(\phi_{20})/r) + \phi_{20}$.

In the same way, we can obtain the necessary condition for RLMA to be in the two-point subprocess of step 2 as

$$\phi_{21} \le \phi \le \frac{L_p(0)}{r} - \frac{L}{2r} + \frac{s_{12}(\phi) - s_{12}(\phi_{20})}{r} + \phi_{20}. \quad (15)$$

With consideration of slippage, the kinematics of RLMA going on stairs can be given by

$$\begin{aligned} x_m &= x_{30} + [r(\phi - \phi_{30}) - s_3(\phi)]\cos\theta_s \\ z_m &= z_{30} + [r(\phi - \phi_{30}) - s_3(\phi)]\sin\theta_s \\ \theta &\approx \theta_s \end{aligned} \quad (16)$$

where $\phi_{30} = \phi_{20} + L_p(0)/r - (L/2r) + \Sigma s_{12} - s_{12}(\phi_{20}) + s_{30}$, $x_{30} = x_{20} + [L_p(0) - (L/2)]\cos\theta_s$, and $z_{30} = z_{20} + [L_p(0) - (L/2)]\sin\theta_s$.

Since step 4 starts when the chassis center passes over the edge of the last stair, from Fig. 2(f) and (16), the necessary condition for RLMA to be in step 3 can be derived by

$$\phi_{30} \le \phi \le \phi_{30} + \frac{n_s b}{r\cos\theta_s} - \frac{L_p(0)}{r} + \frac{\Sigma s - \Sigma s_{12} - s_{30}}{r}. \quad (17)$$

From Fig. 2(b), we can obtain the geometry constraints for successful alternation of track–stair contact points as follows:

$$\frac{2b}{\cos\theta_s} - r\tan\theta_s \le L_p(0) + \frac{L}{2} < \frac{3b}{\cos\theta_s} - r\tan\theta_s. \quad (18)$$

From (18), the necessary condition for two-point interactions of step 3 before climbing the last stair is as follows:

$$\begin{aligned} &\frac{L_p(0) + s_3(\phi)}{r} + \frac{x_s + (k-1)b - x_{30}}{r\cos\theta_s} + \phi_{30} < \phi \\ &< \frac{s_3(\phi)}{r} + \frac{x_s + (k+2)b - x_{30}}{r\cos\theta_s} - \tan\theta_s - \frac{L}{2r} + \phi_{30} \end{aligned} \quad (19)$$

where $k = \lceil (x_m - L_p(0)\cos\theta_s - x_s)/b \rceil < n_s - 1$ is the number of the lowest stair contacting with the tracks.

In the same way, we can obtain the necessary condition for three-point interactions of step 3 as follows:

$$\begin{aligned} &\frac{s_3(\phi)}{r} + \frac{x_s + (k+2)b - x_{30}}{r\cos\theta_s} - \tan\theta_s - \frac{L}{2r} + \phi_{30} \\ &\le \phi \le \frac{L_p(0) + s_3(\phi)}{r} + \frac{x_s + kb - x_{30}}{r\cos\theta_s} + \phi_{30}. \end{aligned} \quad (20)$$

The landing process consists of two subprocesses: as the first subprocess, the pitch joint rotates anticlockwise; in the second subprocess, the driving wheels continue to drive RLMA until it plunges onto the upper floor. The necessary condition for RLMA to be in the first and second subprocesses of step 4 can be given by $\{\phi = \phi_{40}\} \cap \{\pi \le \theta_p \le (10\pi/9)\}$ and $\{\phi \ge \phi_{40}\} \cap \{\theta_p = (10\pi/9)\}$, respectively. Here, ϕ_{40} can be described by $\phi_{40} = \phi_{30} + (n_s b/r\cos\theta_s) + (\Sigma s - \Sigma s_{12} - s_{30}/r) - (L_p(0)/r)$.

From Fig. 2(c), the kinematics of the RLMA in the first subprocess of step 4 can be derived as follows:

$$\begin{aligned} x_m &= x_s + n_s b - L_p(0)\cos\theta_s - L_p(\theta_p)\cos(\theta_p + \theta) \\ z_m &= n_s h + \frac{r}{\cos\theta_s} - L_p(0)\sin\theta_s - L_p(\theta_p)\sin(\theta_p + \theta) \\ \theta &= \theta_s - \arctan\left\{\frac{L_p(\theta_p)\sin\theta_p}{L_p(\theta_p)\cos\theta_p - (L/2)}\right\}. \end{aligned} \quad (21)$$

Similarly, the kinematics of RLMA in the second subprocess of step 4 can be described as follows:

$$\begin{aligned} x_m &= x_{41} + r(\phi - \phi_{40})\cos\theta_s \\ z_m &= z_{41} + r(\phi - \phi_{40})\sin\theta_s \\ \theta &= \theta_{41} \end{aligned} \quad (22)$$

where x_{41}, z_{41}, and θ_{41} can be derived by substituting $\theta_p = 10\pi/9$ into (21).

Remark 4: The number of track–stair contact points are assumed to be two or three, which is guaranteed by (18). Since most of the stairs are designed in regular dimension, such irregular stairs as disobeying the constraints (18) are not discussed in this paper. Furthermore, the measured rotating angles ϕ may be calibrated during the course of nose-line climbing, especially for a long stairway. In such a case, ϕ_{30}, x_{30}, and z_{30} should be replaced by the rotating angle coordinates of the preceding calibration point in (16), (19), and (20).

B. Track–Stair Interactive Force Analysis

The tractive forces between tracks and the terrain are normally composed of the longitudinal and lateral tractive forces [15], which can be represented by

$$\begin{aligned} F_d^x &= \mu_x N_d \left\{1 - \exp\left[-\frac{K_s|\dot{s}_d^x|}{\max\left(|\dot{s}_d^x + r\dot{\phi}|, |r\dot{\phi}|\right)}\right]\right\} \\ &\quad \times \cos[\pi + \arctan 2(\dot{s}_d^y, \dot{s}_d^x)] \\ F_d^y &= \mu_y N_d \left\{1 - \exp\left[-\frac{K_s|\dot{s}_d^x|}{\max\left(|\dot{s}_d^x + r\dot{\phi}|, |r\cdot\dot{\phi}|\right)}\right]\right\} \\ &\quad \times \sin[\pi + \arctan 2(\dot{s}_d^y, \dot{s}_d^x)] \end{aligned} \quad (23)$$

where μ_x and μ_y are the coefficients of friction along the longitudinal and lateral directions, respectively, K_s can be determined by a pull slip test, N_d is the normal force, $\dot{s}_d^x$ and $\dot{s}_d^y$ represent the longitudinal and lateral slip velocities, respectively, and $\dot{\phi}$ is the angular velocity of driving wheels.

The motion of the tracks on the terrain of the lower floor can be treated as pull slip when one grouser has hooked the tread or clutched the riser of the first stair firmly. Furthermore, the slip velocities can be given by $\dot{s}_d^x = -r\dot{\phi}$ and $\dot{s}_d^y = 0$, then

$$F_d = \mu_x N_d [1 - \exp(-K_s)] \quad (24)$$

where F_d is the longitudinal tractive force with the superscript "x" being removed for the convenience of presentation.

The motion resistance can be divided into the internal and external resistances. Since driving torques are not studied in this paper, we only study the external resistances R_d, which can be considered to be proportional to normal loads for running on firm grounds as follows:

$$R_d = f_r N_d \tag{25}$$

where f_r is the coefficient of external motion resistances.

According to the D'Alembert's principle of inertial forces, the RLMA will become an equivalent static system if inertial forces and torques are added to the corresponding COG. Furthermore, from the force and moment equilibrium analysis, the supporting force N_d, the equivalent tractive force F_1, and the equivalent supporting force N_1 can be derived as follows:

$$\begin{aligned}
N_d &= \frac{M_I + F_{IX}\,(h - z_m) - F_{IZ}\,(x_s + b - x_m)}{\{\mu_x\,[1 - \exp(-K)] - f_r\}\,h - [x_s + (L\cos\theta/2) + b - x_m]} \\
F_1 &= F_{IX}\cos\psi + F_{IZ}\sin\psi - N_d\sin\psi \\
&\quad - N_d\{\mu_x\,[1 - \exp(-K)] - f_r\}\cos\psi \\
N_1 &= F_{IZ}\cos\psi - F_{IX}\sin\psi - N_d\cos\psi \\
&\quad + N_d\{\mu_x\,[1 - \exp(-K)] - f_r\}\sin\psi
\end{aligned} \tag{26}$$

where $x_s = d_0 + h_g + r + (L/2) - b$, $\psi = \psi_0 + \theta$, and F_{IX}, F_{IY}, M_I represent the inertial forces along $O_B X_B$, $O_B Z_B$, and the inertial moment around $O_B Y_B$, respectively.

For the one-point subprocess of step 2, N_p, N_1, and F_1 can be calculated in the same way as that in step 1. Assuming that the differences of supporting forces at all the points are consistent, from force and moment equilibrium analysis, N_p, N_1, N_2, and $F_1 + F_2$ for the two-point subprocess of step 2 can be calculated as follows:

$$\begin{aligned}
N_1 &= \frac{\left\{\begin{array}{l}[M_I - r\,(F_{IX}\cos\theta + F_{IZ}\sin\theta)]\,(A-2) \\ \quad + (F_{IZ}\cos\theta - F_{IX}\sin\theta)\,[d_2 - (A-1)\,B]\end{array}\right\}}{(AB - d_1)\,(A-2) + (A+1)\,[d_2 - (A-1)\,B]} \\
N_2 &= \left\{(A+1)\;N_1 - F_{IZ}\;\cos\theta + F_{IX}\;\sin\theta\right\}/\,(A-2) \\
N_p &= \left\{AN_1 - (A-1)\,N_2\right\}/\,\{\cos\theta - k_\mu\sin\theta\} \\
F_{12} &= F_{IX}\;\cos\theta + F_{IZ}\;\sin\theta - N_p\,(\sin\theta + k_\mu\cos\theta)
\end{aligned} \tag{27}$$

where $k_\mu = \mu_x\left(1 - e^{-K}\right) - f_r$; d_1, d_2 can be calculated by substituting $k = 1$ into (32); and d_p, A, B can be detailed by

$$\begin{aligned}
d_p &= \frac{L\cos\theta - \left(L\cos\theta_p + \sqrt{4L_p^2 - L^2\sin^2\theta_p}\right)\cos(\theta_p + \theta)}{2} \\
A &= \frac{1}{\sqrt{b^2 + h^2}}\left\{\left(\frac{L}{2} - r\phi\right)\cos\theta + d_p\right\}\cos\theta + 2 \\
B &= \frac{[\mu_x(1 - e^{-K}) - f_r](z_m - r\cos\theta) - d_p - r\sin\theta}{\cos\theta - [\mu_x(1 - e^{-K}) - f_r]\sin\theta}.
\end{aligned} \tag{28}$$

In Fig. 2(e), letting the summation of forces along $O_m X_m$ and $O_m Z_m$ be zeros yields

$$\begin{aligned}
\sum_{i=1}^{n} F_i &= \frac{1}{2}\left\{F_{IX}\cos\theta + F_{IZ}\sin\theta\right\} \\
\sum_{i=1}^{n} N_i &= \frac{1}{2}\left\{F_{IZ}\cos\theta - F_{IX}\sin\theta\right\}
\end{aligned} \tag{29}$$

where $n = 2$ or $n = 3$ are corresponding to the cases with two or three interactive points of step 3, respectively.

From the force and moment equilibrium analysis with two track–stair interactive points in step 3, N_1 and N_2 can be calculated as

$$\begin{aligned}
N_1 &= \frac{1}{d_2 - d_1}\left\{d_2\left(\sum_{i=1}^{2} N_i\right) - r\left(\sum_{i=1}^{2} F_i\right) + M_I\right\} \\
N_2 &= \frac{1}{d_1 - d_2}\left\{d_1\left(\sum_{i=1}^{2} N_i\right) - r\left(\sum_{i=1}^{2} F_i\right) + M_I\right\}.
\end{aligned} \tag{30}$$

For the case with three track–stair interactive points of step 3, with the assumption that the difference of supporting forces at the three interactive points are consistent, N_1, N_2 and N_3 can be calculated from force and moment's equilibrium as

$$\begin{aligned}
N_1 &= \frac{2}{3}\left(\sum_{i=1}^{3} N_i\right) - N_3 \qquad N_2 = \frac{1}{3}\left(\sum_{i=1}^{3} N_i\right) \\
N_3 &= \frac{1}{d_3 - d_1}\left\{r\sum_{i=1}^{3} F_i - M_I - \frac{d_2 + 2d_1}{3}\sum_{i=1}^{3} N_i\right\}
\end{aligned} \tag{31}$$

where

$$\begin{aligned}
d_1 &= \sqrt{\{x_m - [x_s + kb]\}^2 + [z_m - kh]^2 - r^2} \\
d_2 &= \sqrt{\{x_m - [x_s + (k+1)\,b]\}^2 + [z_m - (k+1)\,h]^2 - r^2} \\
&\quad \times \operatorname{sgn}\{x_m - [x_s + (k+1)\,b] - r\sin\theta_s\} \\
d_3 &= \sqrt{\{x_m - [x_s + (k+2)\,b]\}^2 + [z_m - (k+2)\,h]^2 - r^2}.
\end{aligned} \tag{32}$$

The supporting forces N_1 and N_2 for step 4 can be calculated in the same way as that in step 3, but replacing r with $r + (L/2)\sin(\theta_s - \theta)$ and k with $n_s - 1$.

V. Tipover Stability Analysis and Online Tipover Prediction

The ground and tread (or riser) of the stairs generate unilateral constraints, i.e., they can only provide supporting forces to prevent the grousers from plunging into the terrain but cannot provide pulling forces to prevent them from leaving the contact points. Assuming that the required supporting force N_d, which is necessary to construct a force-balanced system, is negative in Fig. 2(b) and (c), the robot will rotate around the grouser–stair interactive point, so as to fall up into the tread of the first stair. On the other hand, with the assumption that the required

supporting force N_1 is negative, the robot will rotate around the grouser–terrain contact point and fall down from the stair. Furthermore, to ensure that the RLMA is able to climb onto the stairs with limited slippage, F_1/N_1 must meet the firmly hooking condition or the firm clutching condition, as described in Section II. Therefore, the tipover stability criterion for step 1 can be defined by

$$\{N_d \geq 0\} \cap \{N_1 > 0\} \cap \left\{ f_{\min} \leq \frac{F_1}{N_1} \leq f_{\max} \right\} \tag{33}$$

where N_d, N_1, and F_1 can be derived according to the track–stair interactive force analysis method presented in Section IV. The limits $f_{\min}$ and $f_{\max}$ can be determined from Fig. 4 as follows:

$$f_{\min} = \begin{cases} -\dfrac{\cos\theta_s + f_s \sin\theta_s}{\sin\theta_s - f_s \cos\theta_s}, & f_s < \tan\theta_s \\ -\infty, & f_s \geq \tan\theta_s \end{cases}$$
$$f_{\max} = \begin{cases} +\dfrac{\sin\theta_s + f_s \cos\theta_s}{\cos\theta_s - f_s \sin\theta_s}, & f_s < \cot\theta_s \\ +\infty, & f_s \geq \cot\theta_s. \end{cases} \tag{34}$$

The same tipover stability criterion shown in (33) applies to the one-point subprocess of step 2. On the other hand, the tipover stability criterion for the two-point subprocess of step 2 can be defined as follows:

$$\{N_p \geq 0\} \cap \{N_1 > 0\} \cap \{N_2 \geq 0\} \cap \left\{ f_{\min} \leq \frac{F_1}{N_1} \leq f_{\max} \right\} \tag{35}$$

where F_1/N_1 can be derived as follows:

$$\frac{F_1}{N_1} = \begin{cases} \dfrac{F_1 + F_2}{N_1 + N_2}, & k_{\text{rem}} = 0 \\ \dfrac{(F_1 + F_2) - f_s N_2 \operatorname{sgn}(F_1 + F_2)}{N_1}, & k_{\text{rem}} \neq 0. \end{cases} \tag{36}$$

The tipover stability criterion for two-point interactions of step 3 and that for step 4 can be defined as

$$\{N_1 > 0\} \cap \{N_2 > 0\} \cap \left\{ 0 \leq \max\left\{ \frac{F_1}{N_1}, \frac{F_2}{N_2} \right\} \leq f_{\max} \right\} \tag{37}$$

where F_1/N_1 and F_2/N_2 are determined by the track–stair interactions, which may be classified into three different cases: 1) the interactive forces are both hooking forces; 2) the lower track–stair interactive force is hooking force and the higher one is frictional force; 3) the higher track–stair interactive force is hooking force and the lower one is frictional force.

Similarly, the tipover stability criterion for three-point interactions can be defined as follows:

$$\{N_1 > 0\} \cap \{N_2 > 0\} \cap \{N_3 > 0\} \cap \left\{ 0 \leq \max\left\{ \frac{F_1}{N_1}, \frac{F_2}{N_2}, \frac{F_3}{N_3} \right\} \leq f_{\max} \right\}. \tag{38}$$

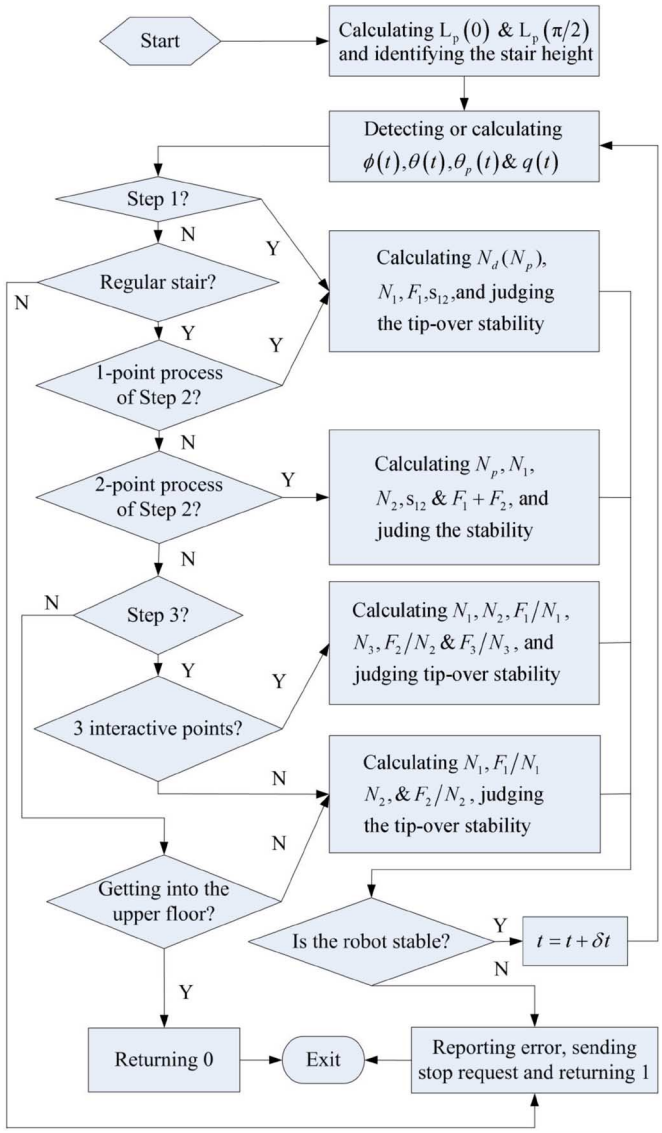

Fig. 5. Online tipover prediction algorithm for RLMA climbing stairs.

The critical condition for the RLMA plunging into the upper level in step 4 is given as follows:

$$\{N_1 = 0\} \cap \{N_2 > 0\} \cap \left\{ 0 \leq \frac{F_2}{N_2} \leq f_{\max} \right\}. \tag{39}$$

On the basis of the track–stair interaction analysis method proposed in the previous sections and the tipover stability criteria derived in this section, an online tipover prediction algorithm is developed, as shown in Fig. 5, which can be used to stop the stair-climbing process before tipover occurs, so as to avoid any damage to the equipment.

In the proposed online tipover prediction algorithm, θ_p and θ may be used together with ϕ to determine which step the RLMA is in, for example, $\{\theta_p \geq 0\} \cap \{\theta \leq \theta_s\} \cap \{\phi \leq \phi_{20}\}$ can be used as a sufficient condition for the RLMA to be in step 1. In step 3, the measurement of ϕ may be calibrated to remove the accumulated errors, especially when incremental encoders are employed. To judge two or three interactive points in step 3,

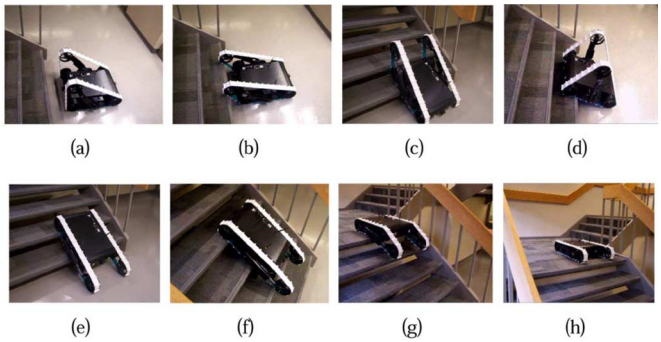

Fig. 6. Snapshots for RLMA climbing stairs: case 1.

TABLE I
DESIGN PARAMETERS FOR RLMA

Parameter	Value	Parameter	Value
L (m)	0.514	$m_m(kg)$	42
L_t (m)	2.046	$m_p\,(kg)$	1.3
h_0 (m)	0.170	$m_f\,(kg)$	1.1
h_g (m)	0.010	l_g (m)	0.2
d_g (m)	0.070	r (m)	0.1

the change of inclination angle detected by the compass can be employed besides (19) and (20). It is observed from experiments that the measured inclination angle changes cyclically with the alternation of track–stair interactive points, which will be detailed in Section VI. Furthermore, the occurrence of slippage can be treated as an indication to change from three-point to two-point interactions. To ensure that RLMA is stopped before tipping over, margins are added to the developed tipover stability criteria, such as δ_N and δ_f in Fig. 5. If the stairway is in such a large dimension that the flippers cannot reach the edge of the second stair, the remote controller can stop the stair-climbing process in step 1.

VI. EXPERIMENTAL RESULTS

To demonstrate the applications of the track–stair interaction analysis method and verify the effectiveness of the tipover prediction algorithm proposed in this paper, experiments are conducted on the RLMA in our laboratory, as shown in Fig. 6. The design parameters for RLMA are listed in Table I.

For RLMA, three drives are dedicated to control the motors and a PC-104 board running QNX is used for high-level control. All the motors are equipped with encoders, and a three-axis compass is equipped to measure the pitch, roll, and yaw of the chassis. Slots around the wheels and the inside of the tracks ensure nonslipping between the wheels and the tracks. The tracks are made of steel reinforced polyurethane, and the elastic deformation in stair climbing is negligible. The communication between the drives and PC-104 is achieved through a controller area network (CAN) bus. An operator control unit (OCU) can be used to send control command to and collect information from RLMA. The communication between OCU and RLMA is achieved via an RF transmitter and a data modem.

To verify the effectiveness of the stair-parameter identification algorithm proposed in Section II, experiments are conducted on a stairway, which has the riser height $h = 18.5$ cm and the tread width of 26 cm, for five times, and the identification results are summarized in Table II. In the experiments, d_0 was selected as 10 cm. The experimental results demonstrate that the proposed stair-parameter identification algorithm can be used to identify the riser height and tread width with an error less than 1 cm. This error is caused by the grousers, which may raise the tracks up.

TABLE II
EXPERIMENTAL RESULTS FOR STAIR-PARAMETER IDENTIFICATION

No.	θ_{p0} $(\circ)$	θ_{p1} $(\circ)$	h (m)	b (m)	θ_s $(\circ)$
1	21.892	6.446	0.192	0.262	36.203
2	22.143	6.574	0.194	0.262	36.587
3	21.332	6.622	0.186	0.259	35.675
4	21.592	7.027	0.189	0.257	36.245
5	22.017	6.838	0.193	0.260	36.634

To demonstrate the effectiveness of the proposed algorithms, the RLMA is controlled to climb stairs with the aid of a remote controller through OCU. Experiments are conducted for three different cases on the aforementioned stairway—stairway 1: in case 1, the stair parameters were identified using the method proposed in Section II, and the corresponding procedure is followed; in case 2, the stair parameters are not identified, and the incline angle is assigned to be 20° so that step 3 starts without hooking the edge of the second stair; furthermore, the tipover prediction algorithm is deactivated in case 2; case 3 is designed to verify the tipover prediction algorithm; the tread width identification and irregular stair detection algorithms are deactivated, and the flippers are not set back until the incline angle for the chassis becomes 60°. For case 1 and case 3, the margins for the tipover prediction algorithm were selected as $\delta_N = 10$ N and $\delta_{fs} = 0.01$, respectively. To further demonstrate the effectiveness of the proposed algorithms, case 1 is repeated on stairway 2 with the following parameters: $\theta_s = 45^\circ$, $h = 20$ cm, and $n_s = 12$.

RLMA climbed onto both the stairways successfully for several times in case 1. The snapshots for case 1 on stairway 1 are shown in Fig. 6. However, RLMA failed to climb onto stairway 1 in the other two cases: in case 2, the tracks slide down from the stairs due to infinite slippage at the end of step 2; the stair-climbing procedure is terminated in case 3 by the tipover prediction algorithm because of $N_d < N_\delta$, as shown in Fig. 7(f).

Slippage and oscillations can be observed in case 1 while going on the nose line. For stairway 1, slippage occurs when one grouser releases from every stair, as shown in the solid line of Fig. 7(c); however, slippage occurs only when one grouser releases from the tread of the odd stairs when climbing stairway 2, as illustrated by the green dashed line in Fig. 7(c). Since release, slippage, and reengagement are finished in a small time period, oscillations of the chassis occur, which can be picked up by the accelerometer in the three-axis compass. As a result, the compass returns strong pulses for both roll and pitch, as shown in Fig. 7(a), which provides a reliable indication for the occurrence of slippage. Therefore, a practical method can be obtained for detecting and measuring slippage of RLMA when

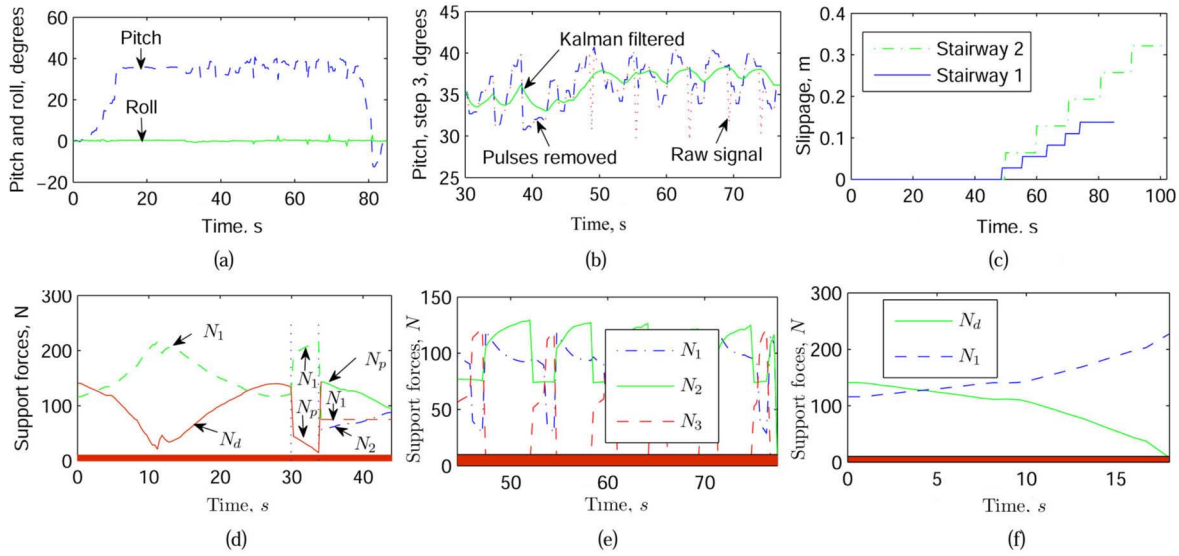

Fig. 7. Experimental results. (a) Pitch and roll from the compass (raw). (b) Pitch angles on the nose line. (c) Slippage. (d) Support forces: steps 1 and 2, case 1. (e) Support forces: steps 3 and 4, case 1. (f) Support forces in case 3.

moving on the nose line as follows:

$$s = \Sigma s_{12} + s_{30} + k{\cdot}s_{3,k} \tag{40}$$

where k is the number of pulses detected by the compass and $s_{3,k} \in \{0, s_{3,k,1}, s_{3,k,2}\}$ has been detailed in Section III-B.

The pitch angles collected by the compass are noisy, especially when moving on the nose line, as illustrated by the dotted line in Fig. 7(b), which cannot be used for online tipover prediction. Besides the aforementioned oscillations, two important factors may cause inclination changes: 1) one grouser may raise RLMA up at the highest track–stair contact point before another one hooking the stair edges firmly and 2) the local deformation of the track at the lowest track–stair contact point makes the practical inclination larger than θ_s.

To predict the tipover stability of RLMA while climbing stairs, the noise caused by oscillations should be removed and the inclination changes caused by grousers and deformation should be retained. The pulses caused by slippage and reengagement can be removed easily by replacing them with the preceding data, as illustrated by the dashed line in Fig. 7(b). Furthermore, to remove the noise caused by oscillations and the other factors as electronic devices, and retain the useful information, a Kalman filter is used as follows [16]:

$$\begin{aligned}
\hat{\theta}\left(k|k-1\right) &= \hat{\theta}\left(k-1|k-1\right) \\
P\left(k|k-1\right) &= P\left(k-1|k-1\right) + Q \\
k_g\left(k\right) &= \frac{P\left(k|k-1\right)}{P\left(k|k-1\right)+R} \\
\hat{\theta}\left(k|k\right) &= \hat{\theta}\left(k|k-1\right) + k_g\left(k\right)\left[\theta_m\left(k\right) - \hat{\theta}\left(k|k-1\right)\right] \\
P\left(k|k\right) &= \left[1 - k_g\left(k\right)\right] P\left(k|k-1\right)
\end{aligned} \tag{41}$$

where $\hat{\theta}$ represents the filtered pitch angle, $k \in [1, \ldots, N]$ with N the total number of sampling points, $Q = 0.1$ and $R = 8$ represent the process noise covariance and the measurement noise covariance, respectively, k_g denotes the Kalman gain, θ_m is the measured pitch angle from the compass (with the pulses removed), $\hat{\theta}\left(0|0\right) = 35$, and $P\left(0|0\right) = 10$.

To avoid unnecessary duplication, only experimental results for stairway 1 are presented in Fig. 7. The filtered pitch angles are compared with the raw pitch signal collected from the compass and those with pulses removed in Fig. 7(b). Time-varying supporting forces in case 1 are given by Fig. 7(d) and (e); and the supporting forces in case 3 are shown in Fig. 7(f).

The experiments have confirmed that stair-parameter identification is crucial for RLMA to climb stairs successfully. In Fig. 7(c), the slip ratio is $\Sigma s/n_s\sqrt{b^2+h^2} \approx 6\%$ for stairway 1 and $(\Sigma s/n_s\sqrt{b^2+h^2}) \approx 9.5\%$ for stairway 2, which cannot be neglected in practical applications. The experiment for case 2 presents an example of sliding down from the stairs due to infinite slippage. In the same way, if the left side of the geometry constraints given by (18) are disobeyed, RLMA will get into the same situation as in case 2. From the experimental result of case 3, we can see that the proposed tipover prediction algorithm can help stop RLMA on time to avoid tipping over.

Remark 5: Even though presented on the basis of a specific self-reconfigurable tracked mobile robot, RLMA, the proposed firm-hooking, firm-clutching, and nonslipping conditions, the slippage and interactive force analysis methods and the tipover stability criteria, and prediction algorithm are general, and can be used for any tracked mobile robots climbing stairs with little modification.

VII. Conclusion

In this paper, track–stair interactions were analyzed systematically and conditions for firm-hooking, firm-clutching, and nonslipping were presented for a self-reconfigurable tracked mobile robot climbing stairs. The stair-climbing process is divided into four steps, and tipover stability criteria were derived for each step, with consideration of the track–stair interactions.

Furthermore, an online tipover prediction algorithm was developed. Experiments were conducted, and the effectiveness of the proposed algorithms were demonstrated with experimental results. As the first attempt to analyze track–stair interactions, this paper has laid a solid foundation for further investigations on this important topic. Active tipover avoidance control, automatically tipover recovery from instable situations, and autonomous control for tracked mobile robots climbing stairs form promising topics for future research.

REFERENCES

[1] P. Ben-Tzvi, S. Ito, and A. A. Goldenberg, "Autonomous stair climbing with reconfigurable tracked mobile robot," in *Proc. IEEE Workshop Robot. Sens. Environ.*, Ottawa, ON, Canada, Oct. 2007, pp. 1–6.

[2] J. Liu, Y. Wang, S. Ma, and B. Li, "Analysis of stairs-climbing ability for a tracked reconfigurable modular robot," in *Proc. IEEE Int. Workshop Saf., Sec. Rescue Robot.*, Japan, Jun. 2005, pp. 36–41.

[3] R. Morales, V. Feliu, A. Gonzalez, and P. Pintado, "Kinematic model of a new staircase climbing wheelchair and its experimental validation," *Int. J. Robot. Res.*, vol. 25, no. 9, pp. 825–841, Sep. 2006.

[4] C. L. Shih, "Ascending and descending stairs for a biped robot," *IEEE Trans. Syst., Man, Cybern. A, Syst. Humans*, vol. 29, no. 3, pp. 255–268, May 1999.

[5] C. Grand, F. Benamar, F. Plumet, and P. Bidaud, "Stability and traction optimization of a reconfigurable wheel-legged robot," *Int. J. Robot. Res.*, vol. 23, no. 10/11, pp. 1041–1058, Oct./Nov. 2004.

[6] H. B. Brown, Jr., J. V. Weghe, C. A. Bererton, and P. K. Khosla, "Millibot trains for enhanced mobility," *IEEE/ASME Trans. Mechatronics*, vol. 7, no. 4, pp. 452–461, Dec. 2002.

[7] A. I. Mourikis, N. Trawny, S. I. Roumeliotis, D. M. Helmick, and L. Matthies, "Autonomous stair climbing for tracked vehicles," *Int. J. Robot. Res.*, vol. 26, no. 7, pp. 737–758, Jul. 2007.

[8] J. D. Martens and W. S. Newman, "Stabilization of a mobile robot climbing stairs," in *Proc. IEEE Int. Conf. Robot. Autom.*, San Diego, CA, May 1994, pp. 2501–2507.

[9] E. T. Esfahani and M. H. Elahinia, "Stable walking pattern for an sma-actuated biped," *IEEE/ASME Trans. Mechatronics*, vol. 12, no. 5, pp. 534–541, Oct. 2007.

[10] E. G. Papadopoulos and D. A. Rey, "The force-angle measure of tipover stability margin for mobile manipulators," *Vehicle Syst. Dyn.*, vol. 33, no. 1, pp. 29–48, Jan. 2000.

[11] Y. Li and Y. Liu, "Kinematics and tipover stability analysis for the mobile modular manipulator," in *Proc. Inst. Mechan. Eng. C, J. Mechan. Eng. Sci.*, Mar. 2005, vol. 219, no. 3, pp. 331–343.

[12] D. A. Rey and E. G. Papadopoulos, "On-line automatic tipover prevention for mobile manipulators," in *Proc. IEEE/RSJ Int. Conf. Intell. Robot. Syst.*, France, Sep. 1997, pp. 1273–1278.

[13] Y. Li and Y. Liu, "Real-time tipover prevention and path following control for redundant nonholonomic mobile modular manipulators via fuzzy and neural-fuzzy approaches," *Trans. ASME, J. Dyn. Syst., Meas., Control*, vol. 128, no. 4, pp. 753–764, Dec. 2006.

[14] (2008). [Online]. Available: http://www.esit.com/mobileRobots.php

[15] Y. Liu and G. Liu, "Kinematics and interaction analysis for tracked mobile manipulators," in *Proc. IEEE/RSJ Int. Conf. Intell. Robot. Syst.*, San Diego, CA, USA, Oct. 2007, pp. 267–272.

[16] G. Welch and G. Bishop. (2006). An introduction to the Kalman filter. [Online]. Available: http://www.cs.unc.edu/welch/kalman/kalmanIntro.html

Yugang Liu received the B.E. degree from the University of Science and Technology, Beijing, China, in 1999, the M.S. degree from Beijing University of Posts and Telecommunications, Beijing, in 2002, and the Ph.D. degree (with honors) from the University of Macau, Macao, China, in 2006.

He is currently a Postdoctoral Research Fellow in the Department of Aerospace Engineering, Ryerson University, Toronto, ON, Canada. His current research interests include modeling and intelligent control of nonholonomic wheeled mobile manipulators, slippage and track–terrain interaction analysis for tracked mobile robots, as well as tipover prediction and prevention for tracked mobile manipulators.

Guangjun Liu (M'99–SM'08) received the B.E. degree from the University of Science and Technology of China, Hefei, China, in 1984, the M.E. degree from the Chinese Academy of Sciences, Shenyang Institute of Automation, Shenyang, China, in 1987, and the Ph.D. degree from the University of Toronto, Toronto, ON, Canada, in 1996.

He is currently an Associate Professor and Canada Research Chair in Control Systems and Robotics in the Department of Aerospace Engineering, Ryerson University, Toronto. He was a Systems Engineer and the Design Lead for Honeywell Aerospace Canada on the Boeing X-32 program from 1997 to 1999. During 1996, he was a Postdoctoral Fellow at Massachusetts Institute of Technology, Cambridge. He has authored or coauthored more than 100 papers in international journals and conference proceedings. His current research interests include control systems and robotics, particularly in modular and reconfigurable robots, mobile manipulators, and aircraft systems.